Toward Standardization of Phasor Near-field OTA Testing for Connected Devices – How RF Phasor Arrays Enable Augmented Measurements

Rudy Bagheriasl

ART-Fi

Orsay, France
rudy.bagheriasl@art-fi.eu

Marylène Cueille

LEAT

Sophia Antipolis, France
marylene.cueille@univ-cotedazur.fr

Thomas Strub

AxesSim

Illkirch-Graffenstaden, France
thomas.strub@axessim.fr

Laurence Richard

ART-Fi

Orsay, France
laurence.richard@art-fi.eu

Jean-Lou Dubard *LEAT*Sophia Antipolis, France
jean-lou.dubard@univ-cotedazur.fr

Christophe Girard

AxesSim

Illkirch-Graffenstaden, France christophe.girard@axessim.fr

Loide de Nascimento Lopes

LEAT

Sophia Antipolis, France
loide-de-nascimento.lopes@etu.univ-cotedazur.fr

Abdelrahman Ijjeh

LEAT

Sophia Antipolis, France
abdelrahman.ijjeh@univ-cotedazur.fr

Stéphane Pannetrat

ART-Fi

Orsay, France
stephane.pannetrat@art-fi.eu

Abstract—RF phasor arrays, first developed for military radars, were recently adopted in the telecom sector, where they have been standardized for Specific Absorption Rate (SAR) measurements. Their utilization for Over-the-Air (OTA) testing addresses the growing demand for accurate characterization of modern wireless devices. This paper presents two physics-based approaches for near-field to far-field transformation using RF phasor probe arrays: the Huygens Box method and the Dipole Synthesis method. Both rely on vector near-field data to calculate far-field radiation patterns without empirical approximations. Measurement results for multi-beam antenna arrays and wideband antennas show strong agreement with anechoic chamber references and simulations, confirming the reliability of the two methods. Besides, equivalent source models derived from these measurements can be integrated into electromagnetic simulations to assess device performance in complex environments, including but not limited to SAR calculation in human voxel models. Preliminary results demonstrate the potential of augmented OTA measurements and highlight the importance of standardization to ensure consistency, comparability, and industry-wide adoption.

Keywords—RF Phasor Arrays, Near-field OTA Measurements, Augmented Measurements, Huygens Box, Dipole Synthesis, EMF Exposure, Standardization, Radiation Pattern.

I. INTRODUCTION

The rapid evolution of wireless technologies, from 5G to emerging 6G and IoT networks, has created unprecedented demand for accurate and scalable OTA testing methodologies. Conventional approaches based on anechoic chambers, while widely used, are limited by high cost, long measurement times, and limited flexibility when it comes to assessing advanced antenna utilizations such as beamforming arrays or devices operating in realistic environments, e.g. autonomous vehicles.

RF phasor arrays, originally developed for radar applications in the defence and aerospace industry, offer a promising alternative by enabling planar near-field phasor measurements that can be transformed into far-field radiation characteristics using physics-based calculation principles described in [1] and [2]. Their industrial maturity is already established in SAR assessment [3,4], as the international standard IEC 62209-3 [5], which was harmonized in the European Union in December 2023, provides testing procedures for vector measurementbased systems. JRC also concluded in [6] that IEC 62209-3 appears more efficient for measuring modern wireless devices as it allows for realistic usage conditions and reduced testing time, and it is better suited to keep up with the increasing demands that the ever-evolving radio access technologies place on mobile devices (e.g. multiple simultaneous frequency transmissions, larger bandwidths, etc.) [7,8]. Extending the application of RF planar phasor arrays to OTA measurements represents the obvious next step toward faster, more versatile, and ultimately more accurate electromagnetic field (EMF) exposure evaluation.

In this paper, we present two independent methodologies for near-field to far-field transformation using RF phasor probe arrays: the Huygens Box method [9] and the Dipole Synthesis method [10]. The two techniques enable augmented OTA measurements by using equivalent sources derived from amplitude and phase data measured with a planar near-field phasor, and embedded into electromagnetic (EM) simulations to assess EMF exposure in complex propagation scenarios. Experimental results on beam-switching antenna arrays and ultrawideband antennas validate the accuracy of the two methods

to derive the far-field when compared to the radiation patterns measured in an anechoic chamber. We further illustrate how augmented measurements can be applied to challenging cases such as SAR analysis when a radiating device is placed in proximity to a flat phantom simulating the human body.

II. FROM PLANAR NEAR-FIELD AMPLITUDE AND PHASE MEASUREMENTS TO 3D FAR-FIELD RADIATION PATTERNS

A planar phasor near-field OTA measurement captures both amplitude and phase of the electromagnetic fields over a near-field scan plane. These data are post-processed using physics-based algorithms to compute far-field radiation. The approach is grounded in electromagnetic theory, and excludes any empirical approximations. Two different methods are employed: the Huygens Box method, based on plane-wave decomposition combined with the equivalence principle, and the Dipole Synthesis method, which relies on source basis function decomposition techniques to represent the Device Under Test (DUT) as an equivalent distribution of dipoles.

A. Huygens Box Method

The Huygens Box method employs a closed surface (typically a rectangular cuboid) surrounding the DUT, on which the tangential electric or magnetic fields are measured. Based on the Huygens principle and the uniqueness theorem, the electromagnetic fields outside this volume, including the far-field, can be uniquely derived from these tangential fields. In the current implementation, near-field measurements are carried out using a planar RF phasor probe array immersed in a high-permittivity, lossy dielectric medium [11]. This commercial implementation comprises the ART-MAN2© system and its associated robot, ART-BORG©, as illustrated in Fig. 1.

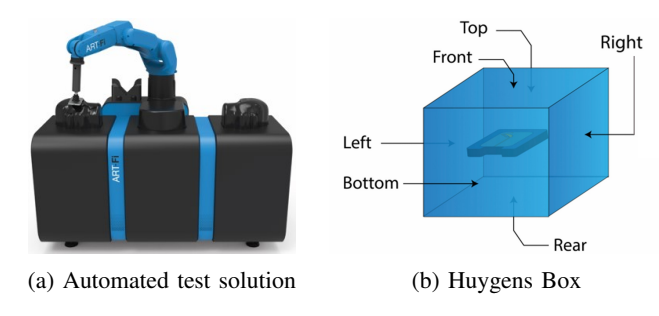


Fig. 1: ART-Fi's technology-leading RF near-field phasor probe array system used to measure the near-field in amplitude and phase on the Huygens Box surrounding the DUT and the SAR in the flat, left head and right head phantoms.

Tested over the flat phantom of ART-MAN2©, the DUT is sequentially positioned in six different orientations relative to the probe array, as depicted in Fig. 2. This gives the EM field distributions on each face of the virtual enclosing box shown in Fig. 1b. For each DUT orientation, plane-wave expansion is applied to transform the measured near-fields from the tissue-simulating dielectric medium into their equivalent free-space representation. Once all six faces are obtained, the full Huygens Box is formed. Finally, standard electromagnetic

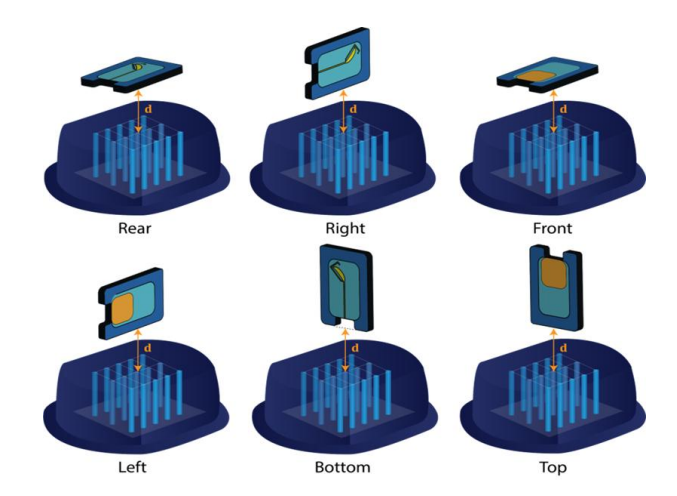


Fig. 2: Planar phasor probe array immersed in the tissue-simulating medium filled flat phantom enabling the measurement of the electric field emitted by the DUT – The six orientations of the DUT relative to the phasor probe array for Huygens Box computation.

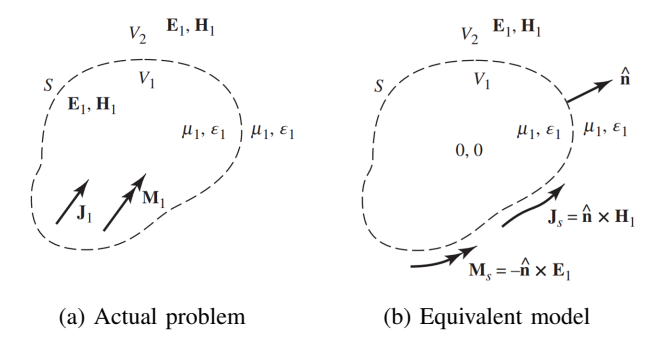


Fig. 3: Description of Love's equivalence principle from [12].

propagation models are used to compute the far-field by applying Love's equivalence principle to the tangential fields to construct equivalent sources for the fields outside the box.

Love's equivalence principle, illustrated in Fig. 3, replaces the actual radiation problem with an equivalent model in which the actual sources J_1 and M_1 inside the imaginary closed surface S are removed. The electromagnetic fields inside S are set to zero and the equivalent surface current densities J_S and M_S are defined by the formulas given in Fig. 3b, where $\hat{\bf n}$ is the unit normal vector pointing outwards from the closed surface S. The electric field at an arbitrarily located observation point outside the closed surface S is given by

$$\mathbf{E} = -j\omega\mathbf{A} - j\frac{1}{\omega\mu\epsilon}\nabla(\nabla\cdot\mathbf{A}) - \frac{1}{\epsilon}\nabla\times\mathbf{F}$$
 (1)

where A and F are the auxiliary vector potentials defined as:

$$\mathbf{A} = \frac{\mu}{4\pi} \int_{V} \frac{\mathbf{J}(\mathbf{r}')e^{-jk|\mathbf{r}-\mathbf{r}'|}}{|\mathbf{r}-\mathbf{r}'|} dV'$$
 (2)

$$\mathbf{F} = \frac{\epsilon}{4\pi} \int_{V} \frac{\mathbf{M}(\mathbf{r}')e^{-jk|\mathbf{r}-\mathbf{r}'|}}{|\mathbf{r}-\mathbf{r}'|} dV'$$
 (3)

with ${\bf r}$ and ${\bf r}'$ representing the observation point and the source point, respectively, and dV' being a differential volume element at the source point ${\bf r}'$. The surface S in Love's equivalence principle is the virtual Huygens Box represented in Fig. 1b as a cuboid for the current implementation.

As a practical example, measurement results obtained using the Huygens Box method are presented for two smart antennas with beam-steering capabilities. Both planar arrays are dual-polarized, which allows operation in either of the two orthogonal linear polarizations. The vertical polarization P1 or the horizontal polarization P2 is excited by feeding either Port 1 or Port 2, respectively. Each antenna has multiple beam states, with peak gain achieved at the 0° beam state corresponding to the broadside direction of the array. Measurements were carried out with the test equipment setup sketched in Fig. 4.

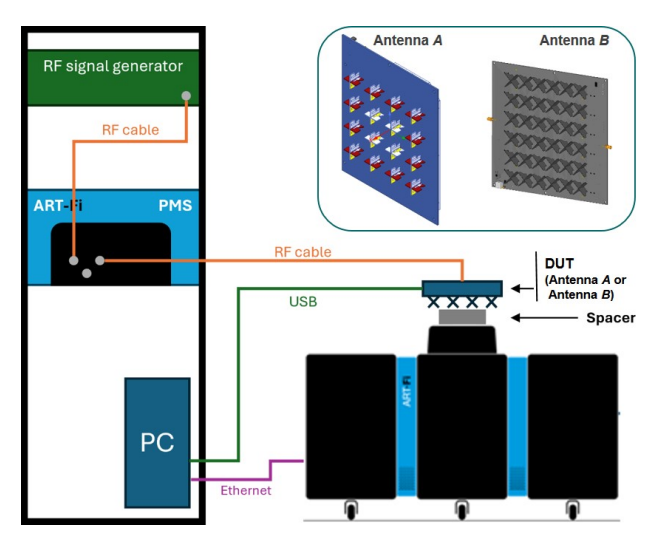


Fig. 4: Test setup with the DUT placed over the flat phantom of ART-MAN2© and fed by a vector signal generator via ART-Fi's power management solution (PMS) integrating amplifiers. The power injected into the DUT is checked with a power sensor before any measurement. The system is calibrated using a reference array antenna for each of the two DUTs.

Antenna A is a 4×4 dual-polarized phased array, whose elementary radiating elements are crossed dipoles operating from 5490-5850 MHz, with a gain of 10 dBi and three beam states (-10°, 0° and +10°) for each polarization. The dimensions of Antenna A are 172 x 140 x 19.2 in mm. Fig. 5 shows the 2D E-plane radiation patterns at 5490 MHz for Antenna A measured with ART-MAN2© and compared to anechoic chamber data. A good agreement is observed for the gain and beamwidth between the two types of measurements. Table I lists the peak gain and beamwidths measured with ART-MAN2© versus the values measured in an anechoic chamber. Good agreement is observed in both the peak gain and the beamwidth between the two series of measured data.

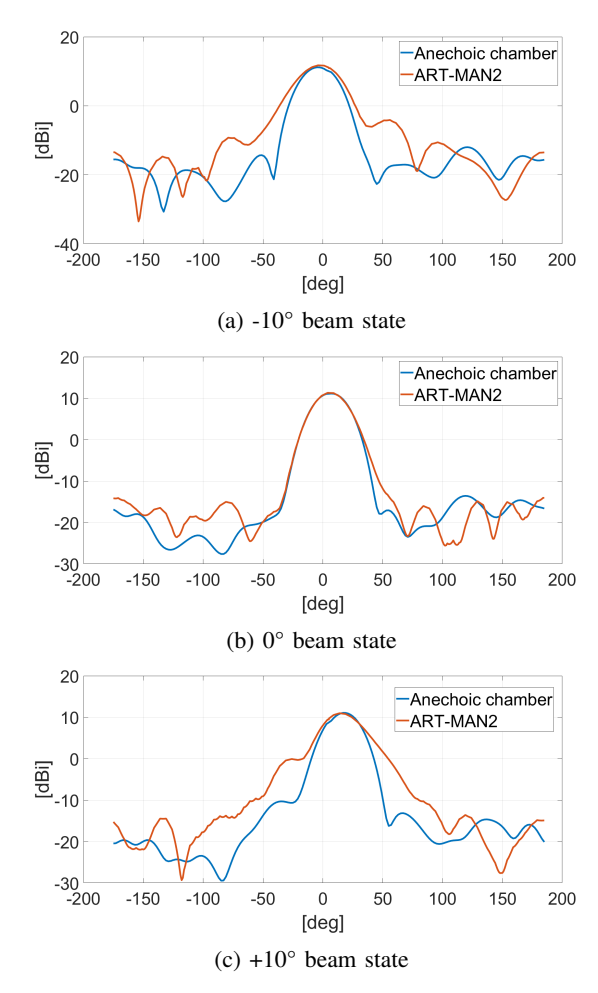


Fig. 5: Measured 2D E-plane radiation patterns at 5490 MHz for the vertical polarization of Antenna A in 3 beam states.

TABLE I: Peak Gains and Beamwidths for Antenna A measured with ART-MAN2© and in an Anechoic Chamber

Frequency	Beam	Peak Gain (dBi) /	Peak Gain (dBi) /
(MHz)	State	Beamwidth	Beamwidth
		[ART-MAN2©]	[Anechoic Chamber]
5490	-10°	9.3 / 31.2°	10.1 / 28.3°
5490	0°	8.4 / 28.3°	10.5 / 29.5°
5490	10°	11.0 / 32.1°	11.1 / 28.9°
5850	-10°	9.3 / 28.2°	10.1 / 28.9°
5850	0°	8.4 / 27.8°	10.5 / 27.6°
5850	10°	9.6 / 29.3°	10.6 / 26.8°

Antenna B is a 6×6 dual-polarized phased array, whose elementary radiating elements are crossed dipoles operating from 3300–4200 MHz, with a gain of 13 dBi and five beam states (0°, ± 15 °, ± 30 °) for each polarization. The dimensions of Antenna B are 252.5 x 270 x 20.5 in mm. The radiation patterns for the two polarizations ± 45 ° are given at 4200 MHz across all beam states in Fig. 6, which demonstrates consistent performance and confirms the capacity of the Huygens Box method to measure different beams with ART-MAN2©.

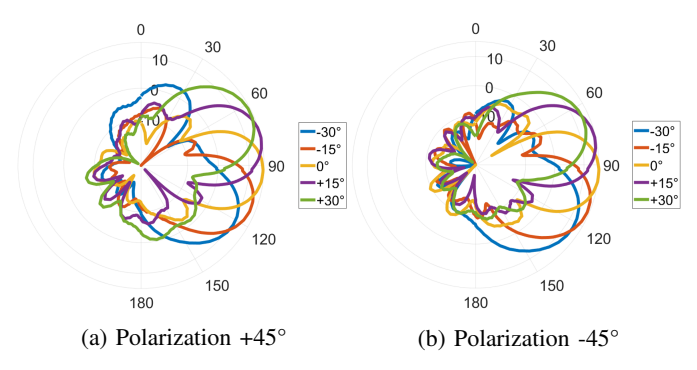


Fig. 6: E-plane radiation patterns for the two polarizations of Antenna B measured with ART-MAN20 at 4200 MHz.

B. Dipole Synthesis Method

Unlike the plane-wave expansion method used for the Huygens Box, the Dipole Synthesis method models the DUT as a 3D grid of equivalent electric and magnetic dipoles using the same near-field phasor measurements. At each grid point, three orthogonal components of electric or magnetic dipoles may be present. In the current implementation, measurements are performed for six different orientations of the DUT using the same planar probe array immersed in a high-permittivity, high-loss medium. Only electric currents are considered in the discrete source set. The electromagnetic field produced by each dipole component at the probe locations is known analytically or via pre-computation. Using the six measured field distributions, an inverse problem is solved to determine the set of dipole sources that best matches the measurements. This dipole set serves as an equivalent source representation of the DUT and can be used to compute its OTA far-field radiation. This is shown in the following equation

$$\mathbf{E}(\mathbf{r}) = \sum_{n=1}^{N} \left[\mathbf{G}(\mathbf{r}, \mathbf{r}'_n) \cdot \mathbf{p}_n \right]$$
 (4)

where \mathbf{p}_n is the electric dipole moment at grid point n, while $\mathbf{G}(\mathbf{r}, \mathbf{r}'_n)$ is the dyadic Green's function relating the dipole source at grid point n to the radiated fields at observation point \mathbf{r} , and N is the total number of dipoles.

The method was applied to an ultra-wideband (UWB) antenna operating from 0.6–3.2 GHz. Amplitudes and phases were acquired in the near-field using ART-MAN2©, and compared to simulation results relative to the UWB antenna in free space using a time-domain numerical method. Fig. 7 shows the antenna model placed on a flat phantom shell. Fig. 8 shows and compares its total radiated power (TRP). A peak occurs near 0.91 GHz, with maxima of $7.28 \times 10^{-11} \, \mathrm{pW}$ for the measurement and $6.17 \times 10^{-11} \, \mathrm{pW}$ for the simulation, corresponding to a relative error of about 19.2%. Between 1 GHz and 2 GHz, the power is relatively stable, varying between $2 \times 10^{-11} \, \mathrm{pW}$ and $4 \times 10^{-11} \, \mathrm{pW}$. Above 2.5 GHz, both curves converge as the TRP decreases toward zero.

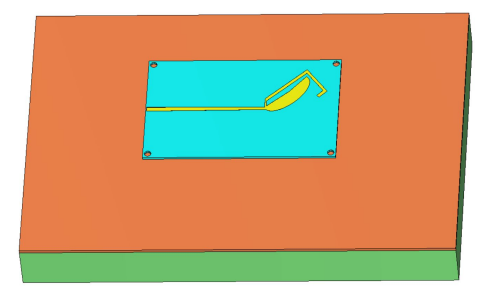


Fig. 7: Model of the UWB antenna over a flat phantom shell with a high permittivity, lossy dielectric medium simulating the human tissue underneath the shell.

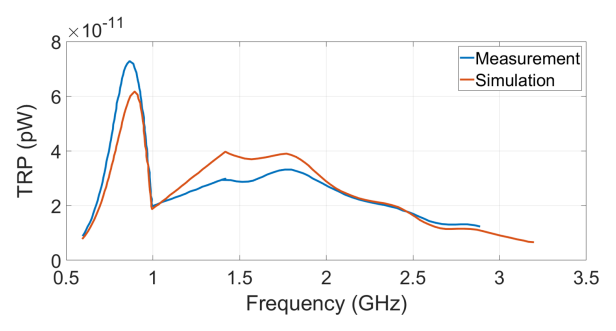


Fig. 8: Total radiated power of the UWB antenna measured with ART-MAN2© using the dipole synthesis method and calculated for the UWB antenna simulated in free space.

Fig. 9 and Fig. 10 show the 3D E-field radiation patterns at 800 MHz and 2470 MHz. At 800 MHz, the 3D shape and spatial distribution of the E-field are captured with high accuracy, although the measurement exhibits a slightly higher maximum amplitude compared to the simulation: 7.5×10^{-11} V/m versus 6.46×10^{-11} V/m. At 2470 MHz, the measurement reproduces the overall spatial distribution and 3D shape well, with minor differences in finer details. The amplitude shows good consistency, with slight variations in maximum and minimum values. The minimum E-field amplitude is approximately 7×10^{-12} V/m for the measurement, compared to 4.96×10^{-12} V/m for the simulation. Conversely, the maximum amplitude is about 4.81×10^{-11} V/m for the measurement, slightly lower than the simulated peak of 5.11×10^{-11} V/m.

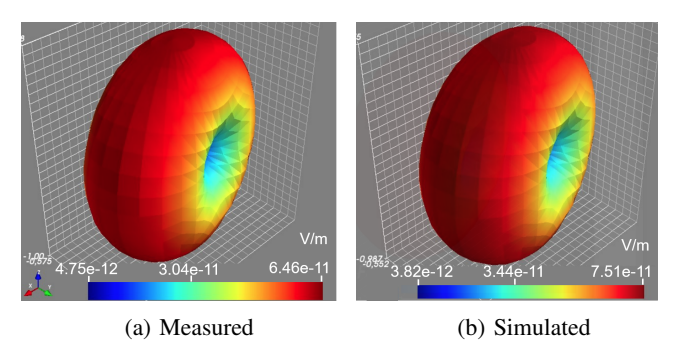


Fig. 9: Measured and simulated 3D E-field radiation patterns of the UWB antenna at 800 MHz.

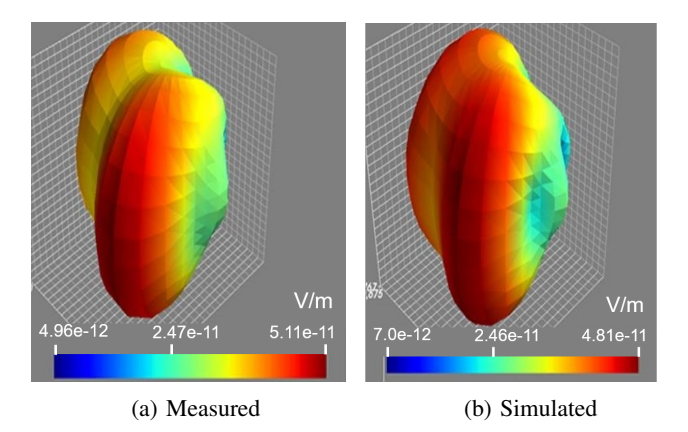


Fig. 10: Measured and simulated 3D E-field radiation patterns of the UWB antenna at 2470 MHz.

III. AUGMENTED OTA MEASUREMENTS

The Huygens Box and Dipole Synthesis methods provide robust frameworks for augmented OTA measurements, in which near-field vector data are transformed into equivalent sources and incorporated into electromagnetic simulation tools. This approach enables accurate evaluation of device performance in realistic environments. As these methods mature, the need for standardized measurement procedures becomes increasingly important. Indeed, standardization enhances consistency and comparability across test setups and organizations and facilitates broader adoption of augmented OTA testing in industrial design and certification workflows. Additionally, Artificial Intelligence (AI) offers potential to support the modeling and simulation phase in complex environments. While AI does not replace physics-based modeling, it can optimize workflows, thus reducing test time and improving scalability.

A. Augmented Measurements using the Dipole Synthesis Method

In this section, the dipole model of the UWB mobile antenna from Fig. 7 is applied in a full-wave 3D simulation [13,14,15]. The UWB mobile antenna is placed next to a head phantom, as shown in Fig. 11. By inserting the dipole model in this environment and adjusting the current amplitudes to correspond to an antenna feed power of 1 W, the specific absorption rate in the orange area and the total radiated power are calculated. SAR measures the rate at which energy is absorbed per unit mass of a human tissue when exposed to a radio frequency electromagnetic field. It is calculated from the electric field in the tissue according to equation (5).

$$SAR = \frac{1}{\rho V} \int_{V} \sigma(\mathbf{r}) |E(\mathbf{r})|^{2} dV$$
 (5)

In this equation, V is the volume of the tissue over which SAR is averaged (e.g. 1 g or 10 g cube) and ρ is the mass density of the tissue, while $|\mathbf{E}(r)|$ is the root mean square electric field strength and σ is the electrical conductivity of the human tissue.

Fig. 12 shows the SAR distribution in the head with a peak value of 93 W/kg, which indicates the potential of this method for evaluating SAR in complex scenarios and for various types of phantoms. Fig. 13 shows the far-field radiation pattern at 910 MHz for the UWB antenna located in free space and placed near the head. One can see the effect of the head, which absorbs the radiation in its direction and reduces the total level. The simulated total radiated power decreases sharply from 371 mW in free space to 119 mW with the head.

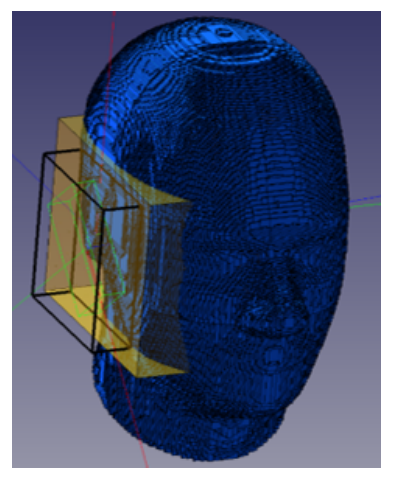


Fig. 11: The UWB mobile antenna's dipole model (green) adjacent to the head phantom (blue). The orange region indicates the SAR calculation zone.

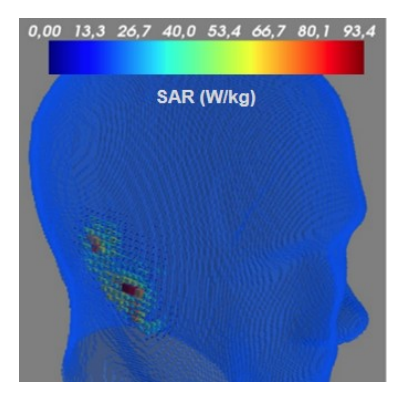


Fig. 12: SAR calculated in the head phantom for the UWB mobile antenna.

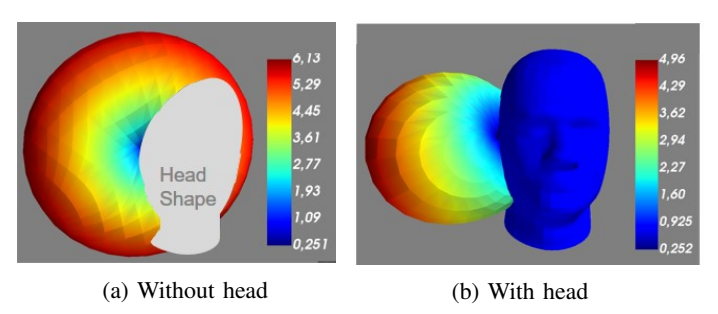


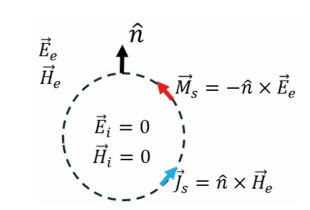
Fig. 13: Simulated modulus of the far-field electric field (3D radiation patterns) for the UWB mobile antenna at 910 MHz.

B. Augmented Measurements using the Huygens Box Method

Augmented OTA measurements can also be performed using the Huygens Box method and a procedure is provided by the authors in [9]. Fig. 14 illustrates the steps for an augmented SAR measurement of a DUT, e.g. a mobile phone:

- 1) Measure the tangential field of the DUT in active propagating mode (i.e. turned on) in free space to obtain \mathbf{E}_e and \mathbf{H}_e (Fig. 14a).
- 2) Apply the equivalence principle to calculate equivalent Huygens sources on the Huygens Box. Using these equivalent sources with an empty box (Fig. 14b) generates the same fields outside the box as in step 1.
- 3) For augmented measurement near complex objects, such as a human head, in proximity to an active mobile phone (Fig. 14c), the equivalent scenario in Fig. 14d is used, where the Huygens sources from Fig. 14b are combined with the DUT (in passive mode, i.e. turned off) inside the Huygens Box.

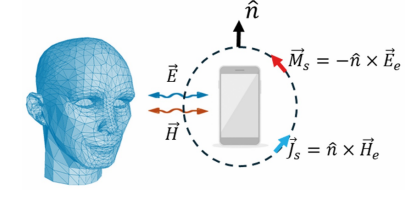




(a) Tangential field measurement with DUT *On*

(b) Equivalent Huygens sources on an empty box





(c) Active DUT (i.e. *On*) close to a human head

(d) Application of Huygens sources with passive DUT (i.e. *Off*)

Fig. 14: The different steps followed to perform an augmented SAR measurement using the Huygens Box method.

IV. CONCLUSION

The Huygens Box and Dipole Synthesis methods have been demonstrated to accurately calculate the radiation characteristics in the far-field (radiation patterns, TRP, gain) by using the amplitudes and phases of the near-field measured with the RF planar phasor probe array system ART-MAN2©. Virtual equivalent sources can be derived from the measured near-field data and incorporated into EM simulation tools. Specifically, it is ART-MAN2©'s unique capability to measure the phase in the near-field that makes it possible now to perform augmented OTA measurements. Standardization of these measurement procedures will be crucial to ensure reproducibility and industrial adoption. Furthermore, AI-assisted simulation and modeling have the potential to optimize workflows, reduce testing time, and improve scalability. Future work will aim to

integrate these tools into standardized certification processes and explore complex scenarios with realistic device usage.

ACKNOWLEDGMENT

The studies presented in this paper were carried out in the framework of two projects: 1) SAM, short for "SAR and Augmented Measurement" funded by the French Defence Innovation Agency (DGA) under the Dual-use Innovation Support Regime (RAPID Program) and 2) CLEAR-ISU, short for "Characterization of Human Exposure to Electromagnetic Fields in Realistic Scenarios", supported by the French National Research Program for Environmental and Occupational Health of Anses (ANSES-23-RF-02).

REFERENCES

- [1] S. Gregson, J. McCormick, and C. Parini, *Principles of planar near-field antenna measurements*. IET, 2007, vol. 53.
- [2] R. F. Harrington, *Time-Harmonic Electromagnetic Fields*. New York: McGraw-Hill, 1961.
- [3] L. Aberbour, O. Jawad, M. Ramdani, P. Giry, and T. Julien, "Efficient experimental assessment of the specific absorption rate (SAR) induced by MIMO wireless communication devices – Application of vector nearfield measurement system," in *IEEE Conference on Antenna Measure*ments & Applications (CAMA). Västerås, Sweden: IEEE, 2018.
- [4] M. Teniou, O. Jawad, S. Pannetrat, and L. Aberbour, "A fast and rigorous assessment of the specific absorption rate (SAR) for MIMO cellular equipment based on vector near-field measurements," in 14th European Conference on Antennas and Propagation (EuCAP). IEEE, 2020.
- [5] "International Standard IEC 62209-3 Measurement procedure for the assessment of specific absorption rate of human exposure to radio frequency fields from hand-held and body-mounted wireless communication devices – Part 3: Vector measurement-based systems (Frequency range of 600 MHz to 6 GHz)," International Electrotechnical Commission (IEC), September 2019.
- [6] C. Chountala, I. Cerutti, J. Ferragut, J. Chareau, J. Bishop, and P. Viaud, "Standards for the Measurement of the Specific Absorption Rate," European Commission, Ispra, Tech. Rep. JRC134671, 2023.
- [7] K. Rachedi, M. Teniou, M. Ramdani, R. Ferrier, S. Pannetrat, and L. Aberbour, "SAR assessment using vector probe array system in the context of RF exposure reduction utilising proximity sensors and timeaveraging technologies," in 15th European Conference on Antennas and Propagation (EuCAP). Online: IEEE, 2021.
- [8] M. Teniou, M. Chamaillard, T. Julien, S. Pannetrat, and L. Aberbour, "A new approach for the evaluation of time averaged SAR of multiple emitting antennas," in *16th European Conference on Antennas and Propagation (EuCAP)*. Madrid, Spain: IEEE, 2022.
- [9] L. D. N. Lopes, A. Ijjeh, S. Mifdal, A. Debard, M. Cueille, J.-L. Dubard, M. Bagheriasl, L. Richard, C. Gouriou, and S. Pannetrat, "Dosimetry computation based on near-field measurements on a Huygens box surrounding the antenna," in 19th European Conference on Antennas and Propagation (EuCAP). Stockholm, Sweden: IEEE, 2025.
- [10] C. Guiffaut, N. Ticaud, and A. Reineix, "Modèle équivalent large bande d'antennes pour implémentation sur porteur," in 18e Colloque International sur la Compatibilité Électromagnétique (CEM), Rennes, France, 2016.
- [11] A. Cozza and B. Derat, "On the dispersive nature of the power dissipated into a lossy half-space close to a radiating source," *IEEE Transactions* on Antennas and Propagation, vol. 57, no. 9, pp. 2572–2582, 2009.
- [12] C. A. Balanis, Antenna Theory Analysis and Design. Wiley, 2016.
- [13] "AXS-SAR: 3D full-wave electromagnetic simulation solution for SAR evaluation," https://www.axessim.fr/axs-sar-specific-absorption-rate.
- [14] X. Romeuf, T. Strub, C. Girard, C. Chanel, A. Guena, N. Ticaud, C. Guiffaut, and A. Reineix, "Évaluation de l'implantation et du découplage d'antennes large bande sur porteur par des modèles équivalents implantés dans une méthode FDTD," in 19e Colloque International sur la Compatibilité Électromagnétique (CEM), Paris, 2018.
- [15] C. Girard, T. Strub, X. Romeuf, C. Guiffaut, and A. Reineix, "Modélisation FDTD des structures antennaires au sein de leur environnement," in *Journées d'Études Compatibilité Radio Électrique (CRE)*, Rennes, France, 2024.